A semiquinone intermediate generated at the Q_o site of the cytochrome bc_1 complex: Importance for the Q-cycle and superoxide production

Jonathan L. Cape*, Michael K. Bowman*†, and David M. Kramer*‡

*Institute of Biological Chemistry, Washington State University, 289 Clark Hall, Pullman, WA 99164-6314; and †Department of Chemistry, University of Alabama, Shelby Hall 113A, P.O. Box 870336, Tuscaloosa, AL 35487-0336

Communicated by Rodney B. Croteau, Washington State University, Pullman, WA, March 20, 2007 (received for review February 2, 2007)

The cytochrome bc_1 and related complexes are essential energy-conserving components of mitochondrial and bacterial electron transport chains. They orchestrate a complex sequence of electron and proton transfer reactions resulting in the oxidation of quinol, the reduction of a mobile electron carrier, and the translocation of protons across the membrane to store energy in an electrochemical proton gradient. The enzyme can also catalyze substantial rates of superoxide production, with deleterious physiological consequences. Progress on understanding these processes has been hindered by the lack of observable enzymatic intermediates. We report the first direct detection of a semiquinone radical generated by the Q_o site using continuous wave and pulsed EPR spectroscopy. The radical is a ubisemiquinone anion and is sensitive to both specific inhibitors and mutations within the Q_o site as well as O_2, suggesting that it is the elusive intermediate responsible for superoxide production. Paramagnetic interactions show that the new semiquinone species is buried in the protein, probably in or near the Q_o site but not strongly interacting with the 2Fe2S cluster. The semiquinone is substoichiometric, even with conditions optimized for its accumulation, consistent with recently proposed models where the semiquinone is destabilized to limit superoxide production. The discovery of this intermediate provides a critical tool to directly probe the elusive chemistry that takes place within the Q_o site.

electron transfer | free radical | photosynthesis | reactive oxygen species | respiration

The cytochrome (cyt) bc_1, b_6f, and related complexes, collectively termed cyt *bc* complexes, are essential components of the respiratory and photosynthetic electron transport chains in mitochondria, many bacteria, and chloroplasts (1–3). These complexes oxidize quinol and reduce one-electron redox carriers while generating an electrochemical gradient of protons, termed the proton motive force (*pmf*), which drives the synthesis of ATP and other bioenergetic processes. The natural substrate is ubiquinol (UQH_2) in the case of the mitochondrial and bacterial cyt bc_1 complexes, and the mobile carrier is cyt *c* in mitochondria or photosynthetic bacteria. The general mechanistic framework for the cyt *bc* complexes is the Q-cycle, first proposed by Mitchell (4–6) and modified by many others (e.g., refs. 7–14).

In "standard" versions of the Q-cycle (2, 9, 15) a unique bifurcated oxidation of QH_2 occurs in the Q_o site, located on the positively charged side (*p*-side) of the membrane. An initial single electron transfer to the "Rieske" 2Fe2S cluster produces a free radical semiquinone (SQ) intermediate (the anionic form or the neutral form, depending on the exact sequence of electron and proton transfers). The Rieske 2Fe2S cluster is the first in a series of carriers, termed the "high potential chain," which in mitochondria and certain bacteria includes cyt c_1 followed by a soluble (or mobile) cyt *c*. Under normal conditions, the SQ intermediate is oxidized by the "low potential chain" leaving a quinone (Q) species in the Q_o site. The first electron carrier in the low potential chain is a *b*-type heme, termed cyt b_L, which reduces the somewhat higher potential cyt b_H, which in turn equilibrates with a Q/SQ couple bound at the quinone reductase (Q_i) site on the negatively charged side (i.e., the *n*-side) of the membrane, opposite the Q_o site. [The cyt b_6f (16–18) and likely the *bc* complexes of certain bacteria possess an additional *c*-type heme in the Q_i site that may participate in reduction of Q.] After two rounds of the bifurcated reaction, two electrons are accumulated on the low potential chain, which fully reduce Q to QH_2 at the Q_i site, with uptake of two protons from the *n*-side of the membrane. Efficient splitting of electrons between the high and low potential chains enforces a net $2H^+/e^-$ proton translocation stoichiometry, thus driving ATP synthesis and other processes.

Recent advances in our understanding of the Q-cycle suggest that it serves a dual role in both energy transduction and the avoidance of deleterious side reactions that lead to oxidative stress (3, 14, 19–21). The Q-cycle is usually highly efficient, but when the bifurcated reaction is partially blocked, "bypass reactions" occur (3, 19, 22) that dissipate energy that could otherwise contribute to ATP production or produce superoxide (19, 22), which has important physiological implications in the progression of aging and neurodegenerative diseases (23–26).

The key question in cyt *bc* complexes is how the Q_o site minimizes bypass reactions while maintaining high flux through the Q-cycle (14, 27, 28). The question is profound because the bypass reactions are vastly more thermodynamically favored (21, 29). Confounding the issue and preventing progress has been the lack of any structural or spectroscopic data on intermediates of the Q_o site. Thus far, x-ray structures (2, 30–33) have not resolved a substrate in the Q_o site, earlier reports of SQ intermediates were found to be insensitive to Q_o site inhibitors (34), and a very recent rapid freeze-quench study (35) found no evidence for SQ intermediates during the uninhibited turnover of the Q_o site. The lack of experimental constraints on the Q_o site intermediates has resulted in a proliferation of mechanistic models, including some that posit highly unusual chemistry or that deviate from the Pauling principle of enzymatic activity (i.e., models that invoke destabilized rather than stabilized reactive intermediates) (3).

An important advance in this area, however, was recently reported by Forquer *et al.* (36), who demonstrated that superoxide production by the yeast bc_1 complex and the Q-cycle share remarkably similar transition states and likely involve the same reactive intermediate species. Thus, identifying the intermediate responsible for superoxide production by the bc_1 complex should

Author contributions: J.L.C., M.K.B., and D.M.K. designed research; J.L.C. and M.K.B. performed research; J.L.C. contributed new reagents/analytic tools; J.L.C., M.K.B., and D.M.K. analyzed data; and J.L.C., M.K.B., and D.M.K. wrote the paper.

The authors declare no conflict of interest.

Abbreviations: cyt, cytochrome; ENDOR, electron nuclear double resonance; SQ, semiquinone; USQ, ubisemiquinone; UQH_2, ubiquinol; cw-EPR, continuous wave EPR; AA, antimycin A.

‡To whom correspondence should be addressed. E-mail: dkramer@wsu.edu.

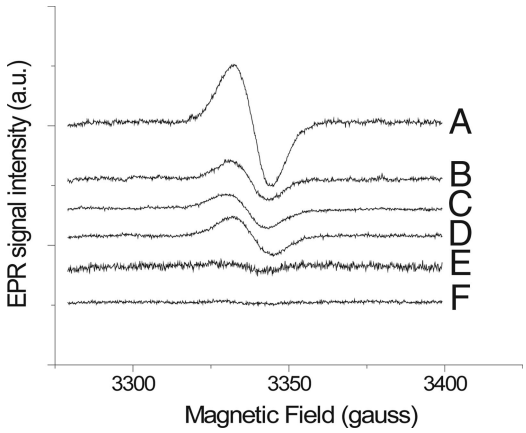

Fig. 1. CW-EPR spectra of SQ species generated from freeze-quenched reactions of AA-inhibited cyt bc_1 with UQH_2. Samples contained 10 μM purified wild-type cyt bc_1, 50 μM UQH_2, and 15 μM AA (trace A); 10 μM purified wild-type cyt bc_1, 50 μM UQH_2, 15 μM AA, and 15 μM stigmatellin (trace B); 10 μM purified H135L cyt bc_1, 50 μM UQH_2, and 15 μM AA (trace C); 10 μM purified H135L cyt bc_1, 50 μM UQH_2, 15 μM AA, and 15 μM stigmatellin (trace D); aerobic 10 μM wt-cyt bc_1, 50 μM UQH_2, and 15 μM AA (trace E); aerobic 10 μM wt-cyt bc_1, 50 μM UQH_2, 15 μM AA, and 15 μM stigmatellin (trace F). The delay time between mixing and freezing was 10 ms. All samples were prepared under anaerobic conditions except where noted. Details of the sample preparation were described in *Materials and Methods*. EPR parameters are as follows: 100-kHz modulation frequency, 5-gauss modulation amplitude, 1-mW microwave power, and 2×10^4 gain. Somewhat different noise levels between traces were caused by increased bubbling of liquid N_2 due to ice buildup in the Dewar insert.

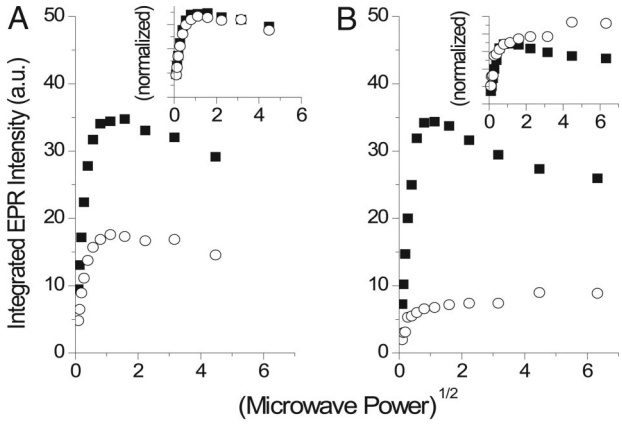

Fig. 2. The effect of Ni(II) on the power saturation properties of +AA and +AA/+stigmatellin SQ signals from freeze-quenched cyt bc_1 samples. (*A*) Power saturation curves from freeze-quenched EPR samples (see *Materials and Methods*) containing cyt bc_1 with AA (filled squares) and cyt bc_1 with AA/stigmatellin (open circles). Power saturation curves shown in *B* are from freeze-quenched cyt bc_1 samples containing AA with 5 mM Ni(II) (filled squares) and AA/stigmatellin with 5 mM Ni(II) (open circles). The *Insets* contain the corresponding data normalized to the amplitudes of the phase saturating at 0.1~0.2 mW.

open the door to identifying the reactive intermediate that drives the Q-cycle and help resolve conflicting Q-cycle models.

Here we present EPR investigations of a Q_o site-generated SQ intermediate detected under anaerobic conditions and show that this stigmatellin and mutation sensitive species is likely the reductant to O_2 under partially inhibited turnover of the cyt bc_1 complex.

Results

Continuous Wave EPR (cw-EPR) Measurements of a New SQ Signal Generated at the Q_o Site. Fig. 1, trace A, shows the 77 K cw-EPR spectrum obtained from a typical anaerobic freeze-quench assay containing 10 μM cyt bc_1 isolated from the photosynthetic bacterium *Rhodobacter capsulatus*, 50 μM UQH_2, and 15 μM antimycin A (AA), with a 10-ms delay between mixing and freezing. In this experiment AA blocked the Q_i site, thus eliminating signals from any stabilized SQ at this site, while preventing reoxidation of the cyt *b* chain (and partially oxidized Q_o site intermediates) through the Q_i site. The free radical signal exhibited a *g*-factor of ≈2.0054 and a line width (11.9 gauss) distinct from that of the narrower Q_i site SQ signal (≈8.0 gauss) (37).

Samples prepared under identical conditions, but with the addition of the Q_o site inhibitor stigmatellin (15 μM) to the assay (Fig. 1, trace B), resulted in an ≈70% decrease in the signal amplitude, indicating that a significant portion of the total radical signal likely originates at the Q_o site of the cyt bc_1 complex. Samples treated with both stigmatellin and AA exhibited $g \approx 2.0058$ and a slight increase in line width from AA-treated samples (12.3 gauss). In the presence of stigmatellin and AA, both Q binding sites are blocked and the remaining SQ signal must be produced through nonenzymatic oxidation of UQH_2. Indeed, signals with similar amplitude are produced in freeze-quenched EPR samples prepared in the absence of cyt bc_1 complex (data not shown).

Identical samples prepared in ambient air rather than argon (Fig. 1, traces E and F) show markedly (>10-fold) decreased amplitudes for both the stigmatellin-insensitive background and Q_o site-generated signals.

Spin counting of the Q_o site-generated SQ (determined from +AA − +AA/+stigmatellin difference spectra), using the SQ generated from chloranil at pH 8.0 as a standard (data not shown), indicated that the SQ_o species is formed in a ratio of ≈0.01–0.1 SQ species per bc_1 monomer depending on the preparation and concentration of enzyme used. These bounds represent the range of values obtained from five separate samples using cyt bc_1 concentrations ranging from 5 to 30 μM.

As an additional test of whether this signal truly originates from the Q_o site of the cyt bc_1 complex, we performed experiments under conditions identical to those described above using purified cyt bc_1 from a strain of *R. capsulatus* in which the primary oxidant to UQH_2 within the cyt bc_1 complex, the Rieske 2Fe2S cluster, is eliminated through mutation of a histidine (H135) ligand to the 2Fe2S cluster to leucine (H135L) (38). The resulting cyt bc_1 complex is identical to the wild type except that the Rieske subunit is not incorporated (38, 39). Fig. 1 (trace C, +AA; trace D, +AA/+stigmatellin) shows that freeze-quenched samples obtained by using the H135L strain were insensitive to stigmatellin treatment. Moreover, the amplitudes of these EPR signals were on the same order as the radical signal obtained in the wild type with stigmatellin freeze-quenched sample shown in Fig. 1. The *g*-factor for these samples was measured to be 2.0061, with a slightly larger line width (13.17 gauss) than +AA samples (Fig. 1, trace A), which was similar to the stigmatellin-treated wild-type samples.

Power Saturation Studies and Paramagnetic Interactions with Ni(II). We used the effect of added paramagnetic Ni(II) on cw-EPR power saturation to probe the accessibility of the SQ species to paramagnetic ions in the aqueous phase of the freeze-quenched samples. These measurements allow an estimation of how deeply buried in a membrane or protein a radical species is by the strength of its magnetic interaction with paramagnetic ions in the bulk solvent (40–42), thus enabling us to distinguish between the SQ species residing in a deeply buried environment, such as the Q_o site, from species generated within or released into the membrane or detergent, which will reside closer to the bulk solvent. Fig. 2 shows representative power saturation curves for

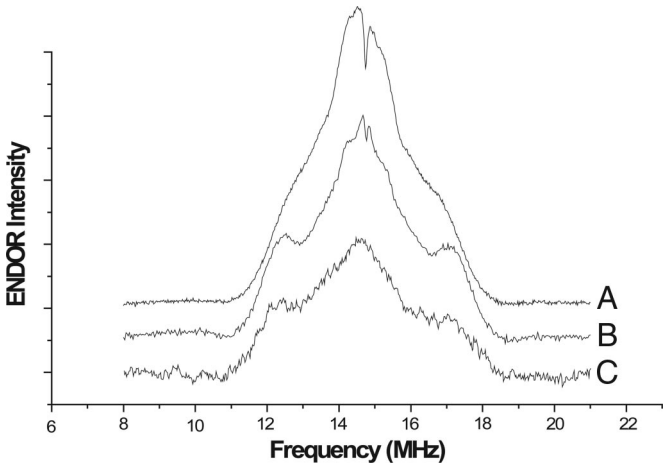

Fig. 3. Proton ENDOR spectra of SQ species generated in aqueous solution, in AA-inhibited cyt bc_1, and in stigmatellin-inhibited cyt bc_1. Chemically produced solution SQ species (trace A) were made in alkaline buffer as described in *Materials and Methods*. (Trace A) USQ produced chemically in aqueous solution. (Trace B) Freeze-quenched species produced with active Q_o site, containing 10 μM purified wild-type cyt bc_1, 50 μM UQH_2, and 15 μM AA. (Trace C) Freeze-quenched species produced with Q_o site blocked by stigmatellin containing 10 μM purified cyt bc_1, 50 μM UQH_2, 15 μM AA, and 15 μM stigmatellin. The intensity of trace C was scaled for comparison purposes. ENDOR was performed at 60 K by using nominal MIMS sequence timing as follows: 16-ns microwave pulses, 120-ns delay between pulses 1 and 2, and 22-μs delay between pulses 2 and 3.

freeze-quenched EPR samples of 18 μM wild-type *R. capsulatus* cyt bc_1 without any additions (Fig. 2*A*) and with 5 mM Ni(II) added to the reaction (Fig. 2*B*). The *Insets* in Fig. 2 show the data normalized to the amplitudes of the phases saturating at ≈0.2 mW. In the absence of Ni(II), both +AA and +AA/+stigmatellin samples exhibit similar power saturation curves indicating partial inhomogeneous line broadening and half saturation points ($P_{1/2}$ = 0.049 and 0.046 mW for +AA and +AA/+stigmatellin-treated samples, respectively), which were slightly higher than those found for the Q_i site-bound SQ species ($P_{1/2} \approx$ 0.02–0.05 mW) (41, 43). Thus, there were no discernable differences in the interactions of the two species with paramagnetic cofactors or other paramagnetic impurities in the sample.

Addition of paramagnetic Ni(II) causes a differential effect on the +AA and +AA/+stigmatellin samples. In the presence of 5 mM Ni(II), the shape of the power saturation curve for the +AA sample remained similar to those without added Ni(II), although exhibiting a small increase in $P_{1/2}$ value (0.088 mW). On the other hand, the power saturation curve for the +AA/+stigmatellin sample shows clear signs of large magnetic interactions with added Ni(II) (see Fig. 2*B Inset* for comparison of normalized curves). This sample exhibits two phases on addition of 5 mM Ni(II), one that saturates at low microwave power (apparent $P_{1/2} \approx$ 0.017 mW) and a second phase that continues to increase in amplitude with increasing power and apparently does not saturate (see Fig. 2*B Inset*, open circles).

These large inhibitor-sensitive changes in the power saturation curve can be explained by overlapping contributions from species in multiple environments exhibiting different saturation and line-broadening properties, one of which exhibits strong dipolar interaction between the $g \approx$ 2.005 spin and the Ni(II) spins, as demonstrated by the continued increase in amplitude at high microwave power. These changes titrate with the concentration of Ni(II) (up to 30 mM; data not shown), with the +AA/+stigmatellin samples having a stronger response to Ni(II) than the +AA samples. Thus, the SQ formed in the +AA/+stigmatellin sample is more exposed to and affected by Ni(II) in the aqueous phase than in the +AA sample.

Pulsed EPR of the Q_o Site Generated SQ. Fig. 3 shows proton electron nuclear double resonance (ENDOR) spectra of a chemically produced ubisemiquinone (USQ) prepared in alkaline solution (pH 11, trace A), the freeze-quenched cyt bc_1 complex treated with just AA (trace B), and the bc_1 complex treated with both AA and stigmatellin (trace C). The magnitudes of the hyperfine couplings identify the species giving rise to the $g \approx$ 2.005 cw-EPR signals in Fig. 3, traces A–C, as USQ anions. Consistent with this interpretation, chemically produced USQ anion yielded an EPR signal with $g \approx$ 2.0056 (data not shown), indistinguishable from that produced at the Q_o site. The ENDOR spectra consist of lines centered at the ^{1}H Larmor frequency of 14.73 MHz flanked by a pair of partially resolved shoulders. The central lines arise from weak hyperfine interactions with protons of the USQ and the surrounding matrix. The larger intensity of the central matrix couplings in the solution USQ species is caused by the high concentration of protons in the aqueous phase around the solution species. The weaker intensity in the +AA and +AA/+stigmatellin samples is attributable to the lower proton concentration in a protein, membrane, or detergent. The ENDOR lines flanking the matrix signal, split by a hyperfine coupling of ≈4.6 MHz for the AA-treated cyt bc_1 sample, are assigned to the protons of the 5-methyl group on the USQ radicals. Neutral SQ radicals, depending on the position of protonation, typically exhibit even larger (10–12 MHz) or much smaller hyperfine couplings to the 5-Me group (44) because of the asymmetry of the singly occupied orbital with respect to the ring substituents (44). The methylene protons of the decyl tail were not resolved in these spectra. The +AA and +AA/+stigmatellin samples (Fig. 3, traces B and C) and solution USQ radical anion (Fig. 3, trace A) show consistent differences in the outer edges of the 5-Me hyperfine line. The solution-generated SQ species (Fig. 3, trace A) exhibits substantial broadening and a smaller splitting (≈4.1 MHz) of the 5-Me couplings compared with the +AA sample, rendering the couplings as little more than shoulders on the central matrix peak. The +AA sample (Fig. 3, trace B) showed noticeably sharper spectral features for both the matrix and 5-Me couplings than the +AA/+stigmatellin sample (Fig. 3, trace C). The electron spin echo envelope modulation (ESEEM) spectra of these freeze-quench samples showed proton ESEEM but no detectable nitrogen ESEEM (data not shown).

Discussion

The key question surrounding the function of the cyt bc_1 complex is how the Q_o site engineers the "bifurcated" reaction, thus storing additional energy as *pmf* while avoiding harmful side reactions. Disruption of the bifurcated reaction results in increased superoxide production, but the intermediate responsible for O_2 reduction is not yet known.

The many various Q-cycle models in the literature (3) differ in one key aspect, the fate and nature of the SQ intermediate at the Q_o site. In some models the SQ is thermodynamically stabilized (45), thus lowering its reactivity with O_2; in other models it is specifically destabilized (3, 36), limiting its reactivity with O_2 by lowering its steady-state concentration. Some models posit that the SQ is shielded from O_2 within the Q_o site (3), while access to the site or its reactivity is proposed to be allosterically (46, 47) or electrostatically (14, 27) gated. Still, other models deny the existence of an SQ intermediate altogether (21).

Previous attempts at trapping EPR-detectable Q_o site SQ species yielded negative or ambiguous results (34, 48) at least in part because of the use of crude preparations and the lack of specific inhibitor controls. Nevertheless, the lack of readily observable SQ was used to support models with an unstable intermediate (9, 49), a tightly bound but EPR-silent SQ (via

spin-coupling to the reduced 2Fe2S cluster) (33), or the complete lack of SQ (21). On the other hand, it is difficult to explain superoxide production by the cyt bc_1 complex without a reactive Q_o site SQ (19, 22), at least under partially inhibited conditions.

In preparations of isolated, AA-treated cyt bc_1 complex, we measure turnover numbers for superoxide of $\approx 10\ s^{-1}$ (20, 22, 36, 50). Assuming a simple second-order process with a maximum second-order rate constant for superoxide production of 10^8 $M^{-1}{\cdot}s^{-1}$ (51) and air-saturated solutions, we predict a minimum steady-state concentration of SQ of ≈4 nM from 10 μM cyt bc_1 complex; this concentration should be detectable by EPR. We thus asked ourselves why it has not been seen. One possibility is that the formation of SQ is more temperature-dependent than its disappearance, i.e., as expected if it occurs near the top of the energy barrier for the overall reaction. In this case we could only hope to observe it with very rapid freeze-quenching, as opposed to the slower cooling tried previously. Also, the SQ is very likely the reductant for O_2 (3, 22) and thus will be sensitive to O_2. To get around these problems, we assayed for SQ by rapid freeze-quench using purified wild-type and mutated cyt bc_1 complex under anaerobic and aerobic conditions. We note that our results are not in contradiction to those of Zhu *et al.* (35), which appeared during revision of our manuscript, because their results were obtained under aerobic conditions in the absence of AA, where we do not expect to observe our SQ species.

Observation of a New USQ Anion and Its Probable Participation in O_2 Reduction. We observe clear evidence from cw-EPR (Fig. 1) and pulsed EPR (Fig. 3) data for a previously unobserved SQ species produced in the Q_o site. The signal is produced in the presence of AA, indicating that is does not occur at the Q_i site. Instead, the signal is sensitive to the Q_o site inhibitor stigmatellin (Fig. 1, traces A and B) and to a mutation (H135L) (Fig. 1, traces C and D) that eliminates the 2Fe2S cluster, indicating that the observed SQ is produced by reaction at the Q_o site (39). Pulsed EPR experiments (Fig. 3) identify the species produced in the Q_o site as a USQ anion, indicating that the QH_2 protons are stripped off faster than the rapid freeze-quench time scale (39). This species exhibits modest difference in line width (≈0.4 gauss) compared with the stigmatellin-insensitive (background) species as well as the radical observed in experiments involving the H135L mutation.

The amplitude of the stigmatellin-sensitive signal is also quite sensitive to O_2 (Fig. 1, traces E and F), indicating that it is very likely the direct O_2 reductant produced during Q-cycle bypass reactions.

The New USQ Species Is Bound, Probably in the Q_o Site. As discussed by Muller *et al.* (22), O_2 reduction by SQ could occur either within the Q_o pocket or after release of SQ from the site into the bulk lipid or detergent environment. We tested these possibilities by probing the proximity of the SQ species to paramagnetic Ni(II) in the aqueous phase. The new SQ species is not greatly affected by paramagnetic interaction with Ni(II), compared with the stigmatellin-insensitive (background) SQ species (Fig. 2). These results indicate that the Q_o site produced SQ is not as accessible to charged ions in the aqueous phase and thus is likely trapped in a protected protein site, probably the Q_o site.

The shapes of the 5-methyl group proton ENDOR lines provide indications about the respective environments of these radicals. In the absence of stigmatellin, the SQ 5-methyl group ENDOR lines are narrower and better resolved than in the other two samples. Such a set of narrow peaks suggests that the ensemble of radicals giving rise to the Q_o site-generated ENDOR signal (Fig. 2, trace B) have similar conformations or environments so that the radicals exhibit a narrow distribution of hyperfine couplings. Both the stigmatellin-insensitive background (Fig. 3, trace C) and the solution SQ species (Fig. 3, trace A) have 5-methyl proton ENDOR lines that are little more than shoulders on the side of the matrix line, suggesting that the radicals are frozen in a variety of conformations and environments, each producing a slightly different hyperfine coupling. The result is a broad ENDOR line for both samples, indicating a wider distribution of hyperfine couplings. We propose that we have trapped significant amounts of the USQ anion before it could escape from the Q_o site, so that it remains in a well defined binding site with limited conformational flexibility.

We found no electron spin echo envelope modulation evidence for a hyperfine coupling between the new SQ species and N-nuclei as might be expected if the SQ was H-bonded to an amide or histidine nitrogen with accompanying SQ spin density on the N (37, 52). Although these couplings have often been difficult to detect, the N-modulation depth in our system appears significantly weaker than for SQs in some related systems, e.g., Q_A in photosystem II (e.g., ref. 53). We also failed to observe broadening or changes in EPR power saturation behavior that might indicate strong coupling of the SQ EPR signal to paramagnetic centers, such as reduced 2Fe2S. Together, these data suggest that, although the SQ is likely bound at or around the Q_o pocket, either it does not have strong paramagnetic interactions with its neighboring cofactors or its interaction is attenuated by binding further away from the Rieske 2Fe2S cluster in the Q_o pocket (e.g., toward the "proximal niche" where myxothiazol binds). Both of these scenarios are consistent with the SQ_o observed here not participating in a strong hydrogen bond with the H161 ligand to the Rieske 2Fe2S cluster, as many Q_o site models hypothesize for Q_o site occupants (e.g., refs. 27 and 28).

Implications for Existing Q_o Site Models and Avenues for the Future. The fact that the SQ_o is sensitive to O_2 indicates that, under aerobic conditions, its accumulation is slower than its consumption, i.e., it reacts irreversibly with O_2 and does not reach quasi-equilibrium with the starting state [QH_2+2Fe2S(ox)]. This observation is at odds with the view (21) that rapid reversibility in the bifurcated reaction insures all states approach quasi-equilibrium on the overall time scale of turnover. Instead, the SQ_o we observe may be a "transient intermediate" that is rapidly consumed during normal turnover via oxidation by cyt b_L or by superoxide production during partially inhibited turnover, and accumulated only when these pathways are blocked (22, 27). Of course, we cannot yet eliminate the possibility that the Q_o site-generated SQ observed here represents a later intermediate in the reaction pathway than the true O_2 reductant formed during uninhibited turnover (36).

The observation of this species provides new limitations on various models of Q_o site chemistry to explain bypass reaction avoidance in the Q-cycle mechanism. Forquer *et al.* (36) have shown that the Q-cycle and superoxide production share an identical or very similar transition states, suggesting that both processes likely involve the same intermediate. Here we show that that this common intermediate is most likely a SQ anion. These data all but disprove the double concerted electron transfer model (21) whereby QH_2 is oxidized in a concerted $2e^-$ and $2H^+$ transfer to the high and low potential chains, completely avoiding SQ formation.

QH_2 oxidation at the Q_o site is pulled forward by the relatively strong oxidant 2Fe2S ($E_{m,7} \approx +300$ mV), and in solution we would expect an equilibrium constant near 1 at neutral pH. In contrast, we trapped only 0.1 to 0.01 SQ per bc_1 monomer under conditions optimized for its accumulation, suggesting that the new Q_o site SQ cannot be one of the highly stabilized SQ species predicted in some models (e.g., ref. 45). This conclusion is also consistent with the observed sensitivity of the SQ to O_2, because stabilizing the SQ will slow its reaction with O_2 (3, 20). Instead, our data are consistent with a model where the Q_o site maintains a highly unstable SQ as a mechanism to limit superoxide

production by decreasing the availability of SQ for the second-order reaction with O_2 (3).

We propose that superoxide production by the cyt bc_1 complex is initiated upon SQ formation and occurs mainly within the Q_o pocket. The rate of superoxide production is thus likely controlled by two factors. First, the redox properties of the SQ/QH_2 couple will control the amount of SQ formed at the site, as demonstrated by the observation that substitution of UQH_2 by rhodoquinol transforms the bc_1 into a "superoxide factory" (54). Second, the Q_o site also likely acts as a barrier to O_2 diffusion into the site, limiting the rate of superoxide production. In this case, changes in the permeability of O_2 into the Q_o site (i.e., its diffusion rate) should have large effects on the maximum rate of superoxide production, and we thus predict that some disease-related mutations of the bc_1 will affect the ability of the Q_o pocket to "shield" the reactive intermediates. This possibility is now directly testable with the discovery of the SQ_o EPR signal.

Overall, the most important implication for the discovery of this signal is the ability to begin testing remaining (previously untestable) Q-cycle models including gated models, destabilized intermediates, and kinetically steered models, all of which make specific predictions for the Q_o site SQ species in terms of thermodynamic and kinetic properties.

Materials and Methods

Chemicals. Decyl-ubiquinone, chloranil, AA, and stigmatellin were obtained from Sigma (St. Louis, MO) and used without further purification. Authentic samples of the SQ derived from decyl-ubiquinone were made in buffer (50 mM Tris/100 mM KCl) made alkaline with NaOH (pH 11). SQ samples from tetrachlorobenzoquinone (chloranil) were prepared in a similar manner, except at pH 8.0, which was sufficiently alkaline to convert nearly all of the chloranil to its SQ form. Final quantification of the chloranil-SQ was made by absorbance (ε_{445} = 9,600 $M^{-1}\cdot cm^{-1}$) (55).

Bacterial Strains, Growth Conditions, and Protein Purification. *R. capsulatus* strains overexpressing wild-type and Rieske H135L mutant complexes were provided as generous gifts from Fevzi Daldal (University of Pennsylvania, Philadelphia, PA); details on the preparation of these strains and the isolation of chromatophore or intracytoplasmic membranes can be found in refs. 38 and 39. All strains were prepared on mineral peptone–yeast extract-enriched media at 23°C under lamp light in anaerobic flasks or in aerobic flasks with shaking at 300 rpm. Purified cyt bc_1 complex was obtained by dodecyl maltoside extraction of chromatophore or intracytoplasmic membranes followed by anion-exchange chromatography (Biogel A) as described (22, 56). Determination of cyt bc_1 concentration was determined spectrophotometrically by using published extinction coefficients (56). Final cyt bc_1 stocks for freeze-quench experiments were diluted to appropriate concentrations (10–50 μM) with 50 mM Tris and 100 mM KCl at pH 8.0.

Preparation of Freeze-Quenched EPR Spectroscopy Samples. For typical assay samples, 100 μM UQH_2 in buffer (50 mM Tris/100 mM KCl, pH 8.0) was reacted with 20 μM purified cyt bc_1 complex in the same buffer, incubated with 30 μM AA or with AA and 30 μM stigmatellin as needed in a 1:1 ratio with a total reaction volume of 200 μl using the rapid freeze-quench apparatus (Model MPS-51; Biologic, Indianapolis, IN) as described in refs. 57 and 58 with modifications. Absorption and EPR spectra showed that the redox carriers of the cyt bc_1 were in their oxidized states before mixing (data not shown). The freeze-quench syringe drive and liquid propane bath were enclosed in a glovebox under an Ar atmosphere with sealed electrical connections to the controller and computer. The reactants were typically incubated on ice under Ar for 2 h before the experiment to generate anaerobic conditions. UQH_2 was diluted into buffer just before loading into the syringe reservoir. The lines leading from the syringes to the mixer and outlet were purged with 150 μl of each reactant over a time period of 50 ms, with the excess taken to waste by suction. A rapid shot of 100 μl from each syringe was routed through the mixer and outlet over a 27-ms time period into a bath of liquid propane. Freeze-quench shots were typically carried out in duplicate into the same liquid propane bath to give a total of 400 μl of frozen material. The liquid propane bath was contained in an aluminum funnel surrounded by a secondary aluminum containment vessel suspended in liquid N_2. Samples for EPR spectroscopy were prepared by packing the freeze-quenched material through a small aperture at the bottom of the aluminum funnel using the shaft of a precooled cotton swab into a 4-mm OD, 4–5 cm long quartz EPR tube sitting in a second liquid propane bath. Two ≈150-μl EPR samples were prepared from each set of freeze-quench shots. The reproducibility of the EPR signal amplitudes between duplicate samples depended on sample packing density and the packing height within EPR tubes. Careful packing and attention to sample height allowed us to achieve good reproducibility in signal amplitudes from replicate samples, with differences between identical samples within the same preparation ranging from 5% to 10% of the total amplitude. The mixing time of the freeze-quench apparatus was calibrated as described (58) using the reaction of myoglobin with azide as a standard.

EPR Spectroscopy. cw-EPR spectroscopy was performed on a Bruker 300E EPR spectrometer with samples at 77 K in a liquid N_2 Dewar insert with the following parameters: 100-kHz modulation frequency, 5-gauss modulation amplitude, 1-mW microwave power, and 2×10^4 gain. A DPPH (2,2-diphenyl-1-picrylhydrazyl) standard was used to calibrate *g*-factors to an accuracy of approximately ±0.0003, considering the signal-to-noise levels of the samples. Lowering the modulation amplitude to 1 gauss did not affect line widths or line shapes in these samples. Spin counting of SQ signals was performed by comparing doubly integrated SQ EPR signals to a standard curve of integrated chloranil SQ signals (10 nM to 10 μM), with all spectra taken at 0.1 mW. Pulsed ENDOR spectra were measured using the Bruker Elexsys 580 spectrometer in the William R. Wiley Environmental Molecular Sciences User Facility at Pacific Northwest National Laboratory using the Mims ENDOR sequence with phase cycling to remove baseline offset and artifacts. ENDOR was performed at 60 K using nominal Mims sequence timing as follows: 16-ns microwave pulses, 120-ns delay between pulses 1 and 2, and 22-μs delay between pulses 2 and 3.

Effect of Ni(II) on Power Saturation Properties. The interaction of the freeze-quench-generated SQ species with added $Ni(II)(NO_3)_2$ was used to probe its environment and solvent accessibility (41, 42, 59). Samples were prepared as described above, except with 5–20 mM Ni(II) added to the protein sample before deoxygenation. We obtained qualitatively similar results using Gd(DTPA) as a paramagnetic relaxation enhancement reagent, but overlap of the $g \approx 2$ component of the Gd(II) EPR signal with the small SQ radical signal complicated these measurements. Thus, only results with Ni(II) are presented here. High concentrations of Ni(II) were found to inhibit AA-resistant quinol oxidation by the cyt bc_1 complex with a K_i of ≈15 mM (data not shown); thus, we restricted Ni(II) to a concentration 5 mM. The cw-EPR spectra of SQ radicals in the presence of added Ni(II) were similar in both shape and intensity to that without Ni(II) but exhibited changes in power saturation properties (see *Results* and *Discussion*). Power saturation curves were plotted from integrated spectra between 0.01 and 40 mW microwave power and fitted as described (41, 42, 59) to obtain

estimates of half saturation values ($P_{1/2}$) and line-broadening parameters.

We thank Dr. Fevzi Daldal for the *R. capsulatus* strains and for stimulating discussions, and we thank Drs. Jason Cooley, Jeffrey Cruz, Antony Crofts, Fevzi Daldal, Atsuko Kanazawa, Fraser Macmillan, Florian Muller, Tomoko Ohnishi, Arthur Roberts, A. William Rutherford, Wolfgang Nitschke, and Sun Un. This work was supported by National Institutes of Health Grant 2 RO1 GM061904 (to M.K.B. and D.M.K.).

1. Crofts AR (2004) *Annu Rev Physiol* 66:689–733.
2. Berry EA, Guergova-Kuras M, Huang LS, Crofts AR (2000) *Annu Rev Biochem* 69:1005–1075.
3. Cape JL, Bowman MK, Kramer DM (2006) *Trends Plants Sci* 11:46–55.
4. Mitchell P (1976) *J Theor Biol* 62:327–367.
5. Mitchell P (1975) *FEBS Lett* 59:137–139.
6. Mitchell P (1975) *FEBS Lett* 56:1–6.
7. Brandt U, Okun JG (1997) *Biochemistry* 36:11234–11240.
8. Crofts AR, Shinkarev VP, Kolling DR, Hong S (2003) *J Biol Chem* 278:36191–36201.
9. Crofts AR, Wang Z (1989) *Photosynth Res* 22:69–87.
10. Crofts AR (2005) in *Biophysical and Structural Aspects of Bioenergetics*, ed Wikstrom M (Royal Soc of Chemistry, Cambridge, UK).
11. Rich P (2004) *Biochim Biophys Acta* 1658:165–171.
12. Trumpower BL (2002) *Biochim Biophys Acta* 1555:166–173.
13. Trumpower BL (1990) *J Biol Chem* 265:11409–11412.
14. Osyczka A, Moser CC, Dutton PL (2005) *Trends Biochem Sci* 30:176–182.
15. Trumpower BL, Gennis RB (1994) *Annu Rev Biochem* 63:675–716.
16. Stroebel D, Choquet Y, Popot JL, Picot D (2003) *Nature* 426:413–418.
17. Cramer WA, Yan J, Zhang H, Kurisu G, Smith JL (2005) *Photosynth Res* 85:133–143.
18. Zhang H, Primak A, Cape J, Bowman MK, Kramer DM, Cramer WA (2004) *Biochemistry* 43:16329–16336.
19. Kramer DM, Roberts AG, Muller F, Cape J, Bowman MK (2004) *Methods Enzymol* 382:21–45.
20. Cape JL, Strahan JR, Lenaeus MJ, Yuknis BA, Le TT, Shepherd JN, Bowman MK, Kramer DM (2005) *J Biol Chem* 280:34654–34660.
21. Osyczka A, Moser CC, Daldal F, Dutton PL (2004) *Nature* 427:607–612.
22. Muller F, Crofts AR, Kramer DM (2002) *Biochemistry* 41:7866–7874.
23. Krantic S, Mechawar N, Reix S, Quirion R (2005) *Trends Neurosci* 28:670–676.
24. Vercesi AE, Kowaltowski AJ, Oliveira HC, Castilho RF (2006) *Front Biosci* 11:2554–2564.
25. Orrenius S, Gogvadze V, Zhivotovsky B (2007) *Annu Rev Pharmacol Toxicol* 47:143–183.
26. Martin GM, Loeb LA (2004) *Nature* 429:357–359.
27. Crofts AR, Lhee S, Crofts SB, Cheng J, Rose S (2006) *Biochim Biophys Acta* 1757:1019–1034.
28. Mulkidjanian AY (2005) *Biochim Biophys Acta* 1709:5–34.
29. Kramer DM, Crofts AR (1993) *Biochim Biophys Acta* 1183:72–84.
30. Kim H, Xia D, Yu CA, Xia JZ, Kachurin AM, Zhang L, Yu L, Deisenhofer J (1998) *Proc Natl Acad Sci USA* 95:8026–8033.
31. Iwata S, Lee JW, Okada K, Lee JK, Iwata M, Rasmussen B, Link TA, Ramaswamy S, Jap BK (1998) *Science* 281:64–71.
32. Hunte C (2001) *FEBS Lett* 504:126–132.
33. Berry EA, Huang LS (2003) *FEBS Lett* 555:13–20.
34. Junemann S, Heathcote P, Rich PR (1998) *J Biol Chem* 273:21603–21607.
35. Zhu J, Egawa T, Yeh S-R, Yu L, Yu C-A (2007) *Proc Natl Acad Sci USA* 104:4864–4869.
36. Forquer I, Covian R, Bowman MK, Trumpower B, Kramer DM (2006) *J Biol Chem* 281:38459–38465.
37. Kolling DR, Samoilova RI, Holland JT, Berry EA, Dikanov SA, Crofts AR (2003) *J Biol Chem* 278:39747–39754.
38. Valkova-Valchanova MB, Saribas AS, Gibney BR, Dutton PL, Daldal F (1998) *Biochemistry* 37:16242–16251.
39. Davidson E, Ohnishi T, Atta-Asafo-Adjei E, Daldal F (1992) *Biochemistry* 31:3342–3351.
40. Oliver ME, Hales BJ (1993) *Biochemistry* 32:6058–6064.
41. Case GD, Ohnishi T, Leigh JS, Jr (1976) *Biochem J* 160:785–795.
42. Galli C, Innes JB, Hirsh DJ, Brudvig GW (1996) *J Magn Reson B* 110:284–287.
43. Ohnishi T, Trumpower BL (1980) *J Biol Chem* 255:3278–3284.
44. Pederson JA (1985) *CRC Handbook of EPR Spectra from Quinones and Quinols* (CRC Press, Boca Raton, FL).
45. Link TA (1997) *FEBS Lett* 412:257–264.
46. Cooley JW, Ohnishi T, Daldal F (2005) *Biochemistry* 44:10520–10532.
47. Covian R, Trumpower BL (2005) *J Biol Chem* 280:22732–22740.
48. de Vries S, Albracht SP, Berden JA, Slater EC (1981) *J Biol Chem* 256:11996–11998.
49. Crofts AR, Guergova-Kuras M, Kuras R, Ugulava N, Li J, Hong S (2000) *Biochim Biophys Acta* 1459:456–466.
50. Sun J, Trumpower BL (2003) *Arch Biochem Biophys* 419:198–206.
51. Afanas'ev IB (1989) *Superoxide Ion: Chemistry and Biological Implications* (CRC Press, Boca Raton, FL).
52. Grimaldi S, MacMillan F, Ostermann T, Ludwig B, Michel H, Prisner T (2001) *Biochemistry* 40:1037–1043.
53. Deligiannakis Y, Boussac A, Rutherford AW (1995) *Biochemistry* 34:16030–16038.
54. Cape JL, Bowman MK, Kramer DM (2005) *J Am Chem Soc* 127:4208–4215.
55. Rathore R, Kochi JK (1996) *J Org Chem* 61:627–639.
56. Ljungdahl PO, Pennoyer JD, Robertson DE, Trumpower BL (1987) *Biochim Biophys Acta* 891:227–241.
57. Appleyard RJ, Evans JNS (1993) *J Magn Reson B* 102:245–252.
58. Appleyard RJ, Shuttleworth WA, Evans JNS (1994) *Biochemistry* 33:6812–6821.
59. Meinhardt SW, Ohnishi T (1992) *Biochim Biophys Acta* 1100:67–74.